Bulletin of the Seismological Society of America, Vol. 93, No. 4, pp. 1679–1690, August 2003

Empirical Corrections for Basin Effects in Stochastic Ground-Motion Prediction, Based on the Los Angeles Basin Analysis

by Claire E. Hruby and Igor A. Beresnev

Abstract Amplification corrections are presented for the finite-fault stochastic ground-motion simulation model; these corrections represent the total effect of the Los Angeles basin on the ground-motion spectra. Spectral amplification ratios were calculated by dividing the observed spectra for the 1994 Northridge and 1987 Whittier Narrows earthquakes, including shear- and basin-generated waves, by the simulated spectra created assuming an average rock-site condition. Smoothed amplification data were plotted above 3D images of the basin revealing a general correlation between the estimated basin depth and total basin amplification for both earthquakes over three frequency ranges: low (0.2–2 Hz), intermediate (2–8 Hz), and high (8–12.5 Hz). The depth-dependent corrections are derived from the regression of the combined data from both earthquakes in order to reduce an uncertainty caused by the azimuth of incoming waves.

Ground-motion duration is defined as the time for 95% of the acceleration spectral energy to pass after the *S*-wave arrival. Due to ambiguity in defining a basin parameter controlling duration, it was impossible to develop a generic equation that would relate the duration ratio (observed/synthetic) to some characteristic of the basin. Users are cautioned, though, that the durations within the basin may be as much as four times longer than the simulated ones.

The procedure is outlined for potential users who wish to use the results of this study in synthesizing more accurate earthquake ground motions, taking into account complicated basin-geometry and near-surface effects. The results are directly applicable to engineering simulation of strong ground motions in a sedimentary-basin environment.

Introduction

Stochastic modeling, in both point-source and finite-fault implementations, has become a popular tool of strong-motion prediction for engineering analyses, especially in the regions with insufficient amounts of instrumentally recorded data (Boore and Atkinson, 1987; EPRI, 1993; Silva *et al.*, 1997; Toro *et al.*, 1997; Atkinson and Silva, 2000; Beresnev and Atkinson, 2002). The stochastic finite-fault modeling technique has been recently developed and validated by Atkinson and Silva (2000) and Beresnev and Atkinson (2001, 2002), as well as validated by other investigators (Hartzell *et al.*, 1999; Berardi *et al.*, 2000; Castro *et al.*, 2001; Iglesias *et al.*, 2002; Roumelioti and Kiratzi, 2002).

One of the main premises of the stochastic method is that the complex path effects, including those of a stratified crustal structure, can be modeled through a semiempirical approach, in which the waves generated at the source are propagated to the observation point using empirically derived models of distance-dependent duration and attenuation. These models are usually obtained from the analysis of regional seismographic data, typically consisting of the records of small earthquakes at rock sites. The salient effects of horizontally stratified crust, including the presence of strong reflections and regional seismic phases, can thus be reasonably well reproduced. To generate a final seismogram at any particular site of interest, the synthetic time history (or spectrum) is multiplied by a desirable site-response function.

This method has not been designed to accurately reproduce ground motions within sedimentary basins, where site effects are not simply reduced to the multiplication by a local response, as illustrated, for example, by Chávez-García and Faccioli (2000) and Makra *et al.* (2001). For example, ground-motion durations can be complicated functions of the distance from the basin edge (e.g., Joyner, 2000). It would be impossible to develop comprehensive theoretical corrections accounting for the basin effects within complex geometries; however, the possibility of using the stochastic method at sedimentary-basin locations would still be desir-

able. Developing such corrections to the synthetic motions empirically is thus the realistic way to proceed.

In the present work, we address the magnitude of the possible corrections and develop the corresponding correction factors for the case of the Los Angeles basin, California, using ground motions from the densely recorded *M* 6.1 1987 (October 1) Whittier Narrows and *M* 6.7 1994 (January 17) Northridge earthquakes. The stochastic finite-fault method, as incorporated in the code FINSIM, has recently been calibrated using multiple rock-site recordings from these events to achieve a statistically near-zero prediction bias for the Fourier and response spectra, in the frequency range from 0.2 to 13 Hz (Beresnev and Atkinson, 2001, 2002). The prediction bias was defined as the ratio of the observed to predicted spectrum, averaged over all modeled stations. Given the availability of this calibrated model, we proceed to the development of the basin-structure corrections as follows.

We use the calibrated model to generate synthetic motions at the sites that are located within the basin. The mismatch (bias) for each station is calculated by dividing the Fourier spectrum of the full trace following the *S*-wave arrival by the simulated spectrum. This mismatch could also be called the spectral amplification ratio, assuming the amplification of the observation relative to the simulation. These ratios are analyzed, as a function of estimated basin depth, in three separate frequency bands: 0.2–2, 2–8, and 8–12.5 Hz (low, intermediate, and high frequencies, respectively). The amplification ratios, appropriately averaged over a number of stations, represent the total correction, which can be viewed as the correction versus the average rock-site condition. Similarly, the ratios can be calculated between the durations observed within the basin and those computed by the simulation model.

All synthetics are generated using the finite-fault radiation simulation code FINSIM (Beresnev and Atkinson, 1998) in the same way as was described by Beresnev and Atkinson (2002) (see Beresnev and Atkinson [2002] for a detailed description of modeling parameters). All input- and output-parameter files, as well as a copy of the code, are freely available from the authors.

One could argue that the results of such a study would only be characteristic of the Los Angeles basin, as reflected in the title of the article. This argument is generally valid; however, one could reasonably assume that the spectral features brought about by the propagation of the edge-generated surface waves into the basin might be quite generic, being only weakly related to the specifics of internal basin structure, since these waves are generated locally at the periphery of the basins. If the distance from the edges to the center is reasonably correlated with depth, as one could assume for "smooth" basin shapes, the captured correction might be roughly applicable to a generic basin. The correction magnitude may also depend on the azimuthal position of the earthquake epicenter relative to the basin (e.g., Bard and Bouchon, 1980a,b; Olsen, 2000); we address this fact by analyzing the data from the two events with very different epicenter locations (although we admit that analyzing just two events may not be representative of the possible total azimuthal variability). By the same token, the spatially variable amplification caused by the impedance gradient across the thickness of the sedimentary cover could be adjusted to a specific basin by modifying the developed corrections proportionally to its impedance contrast. Despite these suggested procedures as to the application of these results to different basins, similar empirical corrections should be developed for the other basins as more earthquake data become available.

We should also point out that the purpose of this study is not to study the amplification effects in Los Angeles basin, which are rather well understood (e.g., Field and SCEC Phase III Working Group, 2000). Our goal is to develop the empirical corrections to ground-motion simulation methods that do not directly take the basin structure into account, in order to make them more accurate within basin geometries. We develop the order of magnitude of these corrections that capture the salient effects. Further studies, carried out over a variety of basin structures where sufficient data may become available, will help clarify the questions raised.

Data and Analysis

By comparing the observed data from the sites within the Los Angeles basin to the synthetic "rock-site" records, following the given algorithm, we have isolated the effects of the basin on both the amplification and duration of seismic waves. The stations used in this study are mapped in Figure 1 and listed in Table 1. All of the stations are operated by either the University of Southern California or the California Division of Mines and Geology (now the California Geological Survey). The stations are classified as generic "rock" (classes A and B) or generic "soil" (classes C and D) according to the Geomatrix scheme; the site-class information was provided by Pacific Engineering and Analysis (courtesy of W. J. Silva). The station classes are listed in Table 1. For the Northridge earthquake, the amplification and duration ratios were calculated for all 53 stations listed in Table 1; 36 of these stations provided ratios for the Whittier Narrows earthquake. The ratios for both events are summarized in Table 2. All records included in the analyses were instrument and baseline corrected. Full traces following the *S*-wave arrival were used in the calculation of spectral-amplification corrections, as described later, which included the effects of both prolonged duration and the spectral energy brought about by basin-generated surface waves, within the frequency band considered. Of the Northridge records, all stations recorded more than 25 sec of data after the *S*-wave arrival, except station MTL for which there were only 20 sec recorded. The traces for the Whittier Narrows earthquake are generally shorter, but all of them exceeded the duration of 16 sec following the *S*-wave arrival.

All data were downloaded from the University of California, Santa Barbara, Strong-Motion Database (http://

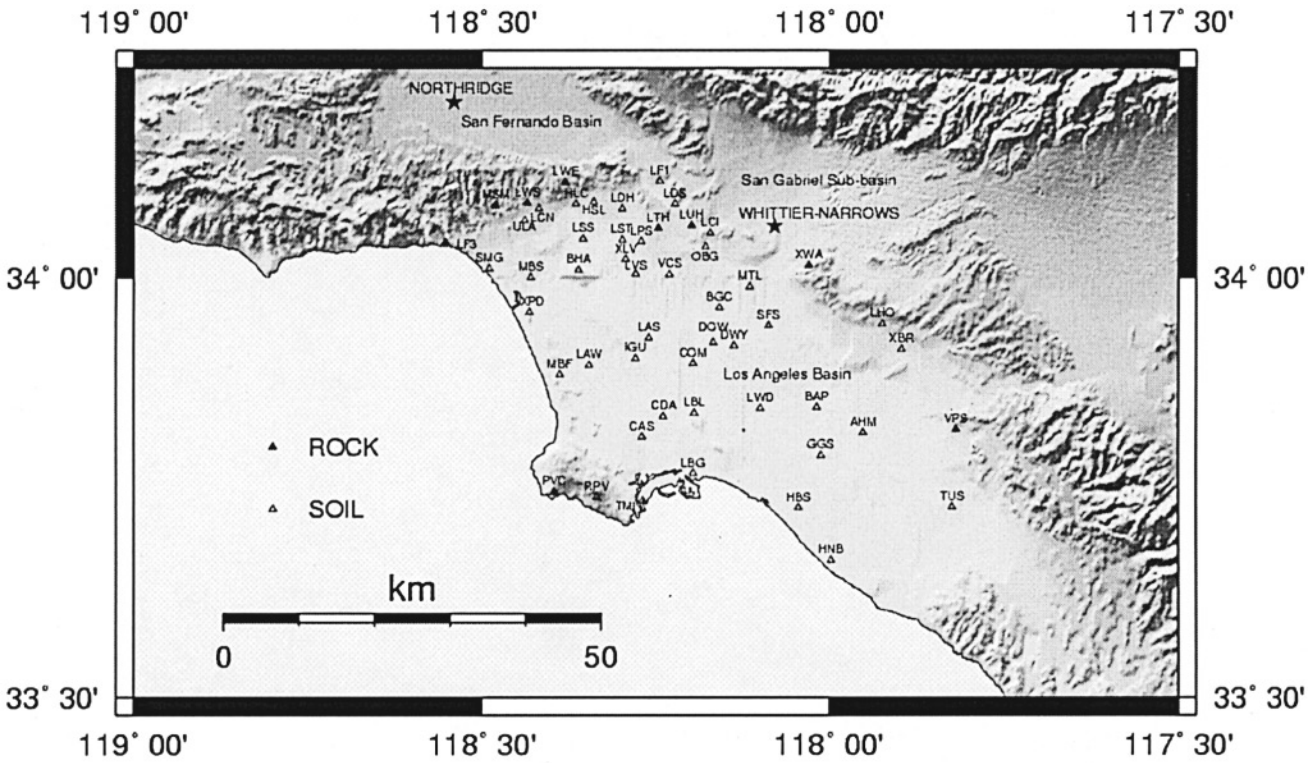

Figure 1. Station map for the Los Angeles basin, including stations for the 1994 Northridge and the 1987 Whittier Narrows earthquakes.

smdb.crustal.ucsb.edu) and resampled to a common sampling interval of 0.02 sec. Our spectral-amplification study is limited to frequencies between 0.2 and 12.5 Hz. The maximum frequency (12.5 Hz) is determined by the 0.2-sec sampling interval of the data. It is unfortunate that the original seismic records did not contain data below the minimum frequency (generally 0.2 Hz, see Table 1), because basin resonances may extend to lower frequencies (Boore, 1999). The exact values of these frequencies for the Los Angeles basin do not appear to have been well identified, and they will certainly depend on the location within the basin. Wald and Graves (1998) infered from their analysis of empirical data and 3D simulations for three Los Angeles basin models that the dominant energies of ground motions were between 0.1 and 0.2 Hz. These frequencies may not be indicative, though, of the true basin resonance, because the analyses were limited to frequencies below 0.5 Hz and the inferred frequencies were for dominant energies, not amplifications. Wald and Graves (1998) did not calculate the frequency-dependent spectral amplifications. Olsen (2000) published the basin amplification values determined from similar 3D simulations for the scenario earthquakes; however, Olsen's amplifications were for peak ground velocity in the frequency band from 0 to 0.5 Hz, not indicative specifically of what frequency primarily contributed to them.

On the other hand, the stochastic-simulation code used in this article has not been tested yet for the frequencies lower than 0.1 Hz (Beresnev and Atkinson, 2002); the frequencies in the band of 0.2–12.5 Hz also cover most of the range of engineering interest.

The Fourier spectral-amplification ratio was calculated between the geometrically averaged horizontal component of observed acceleration records and the random horizontal component of the simulated accelerogram.

Since the rock-site calibrated ground-motion prediction model was used to generate all synthetics, the amplification ratios for stations identified as "rock" hover around unity, as could be expected (see Fig. 3). For soil sites, individual peaks in amplification can be as high as approximately 30. With engineering applications in mind, we used the three frequency bands of 0.2–2, 2–8, and 8–12.5 Hz and calculated average ratios for individual stations over each band. The average amplification ratios range from 0.36 (rock site LWE) to 10.7 (soil site DWY, which lies over the deepest part of the basin).

The basin depth, defined as the depth to the 2.5 km/sec shear-wave velocity isosurface in the Southern California Earthquake Center (SCEC) 3D velocity model of Magistrale *et al.* (2000), was calculated using the Basin Depth Servlet provided on the SCEC web site (www.scec.org:8081/examples/servlet/BasinDepthServlet), which calculates the depth using interpolation on a grid of data points spaced at 400 m. These depths are listed in Table 1. This 3D velocity model is not incorporated into FINSIM simulations; any errors in

Table 1
List of Stations

Station Name	Longitude	Latitude	Location	Agency*	Geomatrix Classification	Estimated Depth (m)	Filter Corners for Horizontal Components (Hz)			
							1994 Northridge Earthquake		1987 Whittier Narrows Earthquake	
AHM	−117.951	33.817	Anaheim	USC		3091	0.200	0.200	0.200	0.400
BAP	−118.018	33.847	Buena Park	USC	D	4472	0.150	0.200		
BGC	−118.158	33.965	Bell Gardens	USC	D	5042	0.150	0.255	0.300	0.080
BHA	−118.361	34.009	Baldwin Hills	CDMG	D	3355	0.080	0.080	0.250	0.250
CAS	−118.270	33.812	Carson: 23536 Catskill Ave.	USC	D	4247	0.130	0.200	0.450	0.150
CDA	−118.239	33.836	Carson: 21288 Water St.	USC	D	3366	0.130	0.300	0.150	0.250
COM	−118.196	33.899	Compton	USC	D	5766	0.200	0.200	0.070	0.225
DOW	−118.167	33.924	Downey	CDMG	D	6095	0.100	0.100	0.250	0.250
DWY	−118.137	33.920	Downey: 12500 Birchdale	USC	D	5613	0.130	0.200	0.090	0.225
GGS	−118.012	33.790	Garden Grove	USC	D	4435	0.150	0.150		
HBS	−118.044	33.727	Huntington Beach	USC	D	3139	0.175	0.130		
HLC	−118.279	33.905	Hollywood	USC	D	1691	0.175	0.110		
HNB	−118.260	33.929	Huntington Beach	CDMG	D	2695	0.100	0.100	0.300	0.300
HSL	−118.346	33.897	LA: Hollywood Storage Lot	CDMG	D	2160	0.080	0.080	0.200	0.200
IGU	−118.196	33.768	Inglewood	CDMG	D	3552	0.080	0.080	0.200	0.200
LAS	−118.194	33.840	LA: 116th Street	CDMG	D	4854	0.080	0.080	0.250	0.250
LAW	−118.271	34.043	Lawndale	USC	D	2705	0.105	0.110	0.275	0.500
LBG	−118.355	34.046	Long Beach: City	CDMG	D	2758	0.150	0.150		
LBL	−118.298	34.045	Long Beach: Rancho	CDMG	D	3596	0.080	0.080	0.250	0.250
LCI	−118.246	34.059	LA: City Terrace	CDMG		2924	0.100	0.100		
LCN	−118.279	34.005	LA: Century City Country Club Nth.	CDMG	D	3248	0.070	0.070	0.300	0.300
LDH	−118.099	33.846	LA: 687 Westmoreland Ave.	USC	D	2475	0.150	0.250	0.250	0.230
LDS	−118.388	33.886	LA: 624 Cypress Ave.	USC	C	2457	0.225	0.250	0.230	0.225
LF1	−118.430	34.001	LA: 3036 Fletcher Dr.	USC	D	548	0.225	0.200	0.225	0.230
LF3	−118.114	33.990	Pacific Palisades	USC	B	348	0.130	0.230	0.350	0.400
LHO	−118.178	34.037	La Habra	USC	C	3296	0.175	0.200	0.200	0.200
LPS	−118.087	33.944	LA: La Pico	CDMG	D	2804	0.100	0.100		
LSS	−118.230	34.004	LA: Saturn St.	USC	D	3310	0.230	0.080	0.175	0.200
LST	−118.293	34.022	LA: St. Thomas	USC	C	2912	0.080	0.130		
LTH	−118.432	33.960	LA: Temple and Hope	CDMG	B	2726	0.100	0.100		
LUH	−118.365	34.088	LA: University Gardens	CDMG	B	2612	0.100	0.100		
LVS	−117.997	33.664	LA: Grand Ave.	USC	D	4664	0.225	0.110	0.225	0.250
LWD	−118.339	34.090	Lakewood: Del Amo	USC	D	5401	0.200	0.225	0.250	0.250
LWE	−118.171	34.053	LA: 8510 Wonderland Ave.	USC	A	310	0.175	0.250	0.500	0.425
LWS	−118.418	34.063	LA: 700 Faring Rd.	USC	B	310	0.175	0.110	0.400	0.300
MBF	−118.298	34.082	Manhattan Beach	USC	C	2181	0.055	0.150	0.300	
MBS	−118.222	34.088	LA: Centinela St.	USC	D	2821	0.105	0.130	0.250	0.200
MSM	−118.244	34.115	LA: 120001 Chalon Rd.	USC	B	310	0.150	0.200	0.550	0.275
MTL	−118.553	34.042	Montebello	USC	D	3909	0.225	0.230		
OBG	−117.924	33.946	LA: Obregon Park	CDMG	D	3284	0.080	0.080	0.200	0.200
PVC	−118.198	34.062	R. Palos Verdes: Hawthorne Blvd.	CDMG	A	0	0.150	0.150		
RPV	−118.380	34.114	Rancho Palos Verdes: Luconia Dr.	USC	C	0	0.175	0.230	0.350	0.425
SFS	−118.435	34.089	Santa Fe Springs	USC	D	4330	0.225	0.200	0.300	0.300
SMG	−118.481	34.086	Santa Monica	CDMG	D	2656	0.070	0.070		
TMI	−118.396	33.746	Terminal Island	USC	D	1631	0.200	0.080	0.170	0.225
TUS	−118.335	33.740	Tustin	USC	D	2431	0.225	0.150		
ULA	−118.490	34.011	LA: UCLA grounds	CDMG		1114	0.080	0.080		
VCS	−118.269	33.736	Vernon	USC	D	4205	0.120	0.225	0.130	0.150
VPS	−117.824	33.728	Villa Park	USC	B	2516	0.650	0.150	0.500	0.450
XBR	−118.439	34.068	Brea	USC	D	3331	0.230	0.200	0.130	
XLV	−117.818	33.821	LA: S. Vermont	USC	D	3944	0.225	0.200		
XPD	−117.896	33.916	Playa Del Ray	USC	D	2005	0.175	0.055	0.300	0.275
XWA	−118.029	34.015	Whittier	USC	B	4409	0.230	0.225		

* USC = University of Southern California; CDMG = California Division of Mines and Geology.

Table 2
Amplification and Duration Ratios (Observed/Synthetic)

	Northridge 1994 Amplification Ratios			Whittier Narrows 1987 Amplification Ratios				
Station Name	Low Frequency (0.2–2 Hz)	Intermediate Frequency (2–8 Hz)	High Frequency (8–12.5 Hz)	Low Frequency (0.2–2 Hz)	Intermediate Frequency (2–8 Hz)	High Frequency (8–12.5 Hz)	Duration Ratios (Northridge)	Duration Ratios (Whit-Narr)
AHM	3.81	2.46	1.36	2.28	1.51	1.81	1.96	2.76
BAP	4.40	3.58	1.57				1.88	
BGC	2.49	2.03	1.94	2.72	1.65	3.06	1.78	2.36
BHA	2.62	2.22	3.63	2.62	2.21	2.83	1.8	2.69
CAS	2.14	1.80	2.51	2.04	1.63	2.92	2.28	4.04
CDA	3.47	2.85	2.88	4.08	2.03	3.41	2.45	2.61
COM	2.71	2.21	2.31	4.76	3.30	5.31	2.21	2.11
DOW	4.07	3.69	2.95	4.68	1.57	2.76	1.62	2.44
DWY	2.84	3.30	2.05	10.67	2.87	2.78	1.59	1.27
GGS	3.84	3.52	2.28				1.54	
HBS	3.46	3.53	3.13				1.58	
HLC	3.22	1.54	1.87				1.44	
HNB	4.07	2.85	2.16	1.39	1.68	2.77	2.65	3.26
HSL	2.88	2.76	4.01	1.94	1.69	4.90	1.13	2.68
IGU	2.06	2.16	2.22	4.03	2.60	5.29	2.47	1.62
LAS	2.34	2.58	3.06	2.95	4.63	4.08	1.57	0.96
LAW	2.17	1.65	2.97	3.21	1.51	2.00	2.23	2.7
LBG	2.66	1.63	1.43				3.65	
LBL	4.01	2.12	1.77	4.82	2.11	2.83	2.85	1.87
LCI	3.11	4.01	6.04				1.14	
LCN	3.38	2.26	2.41	2.06	1.76	3.73	1.28	3.36
LDH	1.85	3.05	1.62	1.35	2.48	2.02	0.88	1.42
LDS	1.84	2.04	2.14	1.99	0.94	1.68	1.09	2.09
LF1	2.28	1.99	1.43	2.31	2.37	1.76	1.07	1.49
LF3	1.56	2.58	2.15	0.70	2.37	1.40	0.94	2.08
LHO	4.49	5.03	2.94	1.78	1.43	1.67	1.59	2.03
LPS	2.17	1.33	1.71				1.74	
LSS	3.95	3.33	2.26	1.67	1.72	3.42	0.93	2.43
LST	2.80	1.79	2.44				2.02	
LTH	2.10	1.34	2.09				1.29	
LUH	2.14	4.00	4.37				1.14	
LVS	2.55	2.52	2.08	2.19	2.54	5.81	1.18	2.13
LWD	4.52	3.88	4.73	5.49	2.40	3.28	1.59	1.83
LWE	0.88	0.83	1.47	0.36	0.51	1.23	0.89	1.02
LWS	2.33	1.62	1.23	0.77	1.12	1.07	0.89	2.15
MBF	2.95	1.36	1.66	3.83	1.30	2.71	2.02	3.88
MBS	3.20	2.97	4.00	1.39	1.15	3.50	1.24	2.62
MSM	2.48	1.09	0.86	0.68	0.62	0.78	0.89	1.63
MTL	2.24	2.57	1.97				1.1	
OBG	2.12	3.25	4.52	4.90	2.79	3.68	0.99	1.61
PVC	1.05	1.19	0.67				1.75	
RPV	2.13	2.35	1.42	2.12	0.66	1.48	0.91	3.85
SFS	2.11	4.25	3.53	3.63	3.00	4.36	1.57	0.79
SMG	3.78	3.38	5.51				1.3	
TMI	3.57	4.49	1.75	2.62	1.70	1.34	1.16	3.31
TUS	2.57	3.50	3.39				1.7	
ULA	2.28	2.31	3.82				0.85	
VCS	1.92	1.85	1.15	3.24	2.53	1.96	1.52	2.32
VPS	1.56	2.06	2.35	1.00	1.34	3.38	1.66	1.68
XBR	3.23	3.23	1.95	1.76	1.31	2.38	1.31	1.69
XLV	1.55	1.17	1.80				1.92	
XPD	2.94	1.29	1.37	1.53	0.97	1.51	2.54	4.34
XWA	1.36	1.13	0.62					

estimated depth are thus introduced into our findings via the equations describing the correlation of amplification with depth.

Results

Data Trends and Localized "Hot Spots"

Three-dimensional images were used to visualize the general trends in inferred amplification corrections and to pinpoint localized amplification "hot spots." Figure 2 shows the 3D plots of smoothed amplification for each frequency range superimposed above a representation of the Los Angeles basin. It is clear that there is a correlation between basin depth and amplification for both earthquakes. Previous studies have also concluded that basin depth is an important factor in determining ground-motion amplitudes (Field and SCEC Phase III Working Group, 2000). The plots in Figure 2 also show variations in the amplification patterns between the two earthquakes; specifically, two high-frequency amplification hot spots appear for the Northridge event, which are not seen in the case of the Whittier Narrows event.

The highest amplification peak occurs over the deepest part of the basin for all three frequency ranges for the Whittier Narrows earthquake. All three Northridge plots also show amplification centered over the deepest part of the basin; however, an additional pocket of high amplification is centered over the Santa Monica region (western end of the plots). Indeed, anomalous amplification was observed in the Santa Monica area during the Northridge event (Porcella *et al.*, 1994; Shakal *et al.*, 1994). The cause of this amplification is thought to be the focusing effect at the basin edge, although there is debate as to the depth causing this effect (Gao *et al.*, 1996; Hartzell *et al.*, 1997; Alex and Olsen, 1998; Graves *et al.*, 1998; Davis *et al.*, 2000).

Another, although weaker, amplification hot spot seen in the Northridge data occurs over the northern edge of the basin, which may be related to the resonance in the smaller San Gabriel subbasin. Such resonance was observed in the results of a 3D finite-difference model for the Northridge earthquake by Olsen (2000) based on the 3D velocity model by Magistrale *et al.* (1998).

The identification of these hot spots is not new. They were previously identified by Hartzell *et al.* (1997) based on the empirical analysis of Northridge mainshock and aftershock data. What is of additional importance for seismic hazard analysis, though, is that the significance of these hot spots appears to depend on frequency and earthquake location. As frequency increases, the amplification hot spots become increasingly dominant. The largest absolute amplification occurs for the high-frequency range of 8–12.5 Hz. This observation is consistent with the results of theoretical focusing by hemicylindrical and hemispherical lenses and the finite-difference simulations of focusing by a 2D curved interface by Davis *et al.* (2000).

The Santa Monica and San Gabriel subbasin hot spots are exceptions to the general depth-dependent trend of the amplification ratios. They may be highly dependent on subtleties of local geology and the azimuth of incoming waves and would be difficult to incorporate in a generic correction model. Because our amplification corrections are averages of the two events with different epicenters, the azimuth-dependent effects are reduced. The creation of localized hot-spot corrections for use with FINSIM or similar programs is beyond the scope of this study; however, such corrections, calculated for a specific structural feature if known, may easily be added to the model.

Amplification Corrections

Prior to the analysis of the entire raw amplification data including both earthquakes, the Northridge and Whittier Narrows amplifications were looked at separately to ensure that both data sets showed correlation between amplification and depth. Both earthquakes showed positive correlation for all three frequency ranges. The absolute amplification values overlapped; however, the Whittier Narrows regressions consistently had steeper slopes than the regressions for the Northridge data.

Combined plots of the amplification ratio versus basin depth, including both events, are shown in Figure 3. Linear regressions were performed for the station amplifications averaged within each frequency range as well as one for the entire frequency range. The equations produced by these regressions are shown in Table 3. All four equations show positive correlation with depth. The low-frequency range shows the best correlation, perhaps due to the contributions from surface waves, primarily formed by low-frequency energy, and due to a lesser effect of small-scale heterogeneities at these frequencies, which are not depth correlated and are impossible to account for in the synthetic model.

The y intercepts for the low-, intermediate-, and high-frequency ranges are 1.42, 1.52, and 1.66, respectively. Theoretically, if the model predicts rock sites accurately, these lines should converge to unity. These regressions, however, are significantly weighted by the stations within the basin. Although one might argue that rock sites should not be included at all in the basin corrections, we prefer to use all of the available stations approximately located within the basin contours, especially because the estimated depth of the basin does not necessarily correlate with the Geomatrix site classification that is based entirely on near-surface geology and because the exact boundary of the basin is not strictly defined. The distribution of sites within the basin is fairly uniform, with the exception of the northwest corner, which has the greatest density of stations.

The corrections presented in Table 3 represent the total amplification ratio at any point within the basin, with respect to the average rock-site condition. Therefore, it is not surprising that the correlation factors (r^2) range from 0.15 to 0.25, reflecting the large amount of scatter. The presence of scatter should be expected, since it involves the presence of amplification hot spots, uncertainty in the calculation of basin depth, and variable response of near-surface deposits,

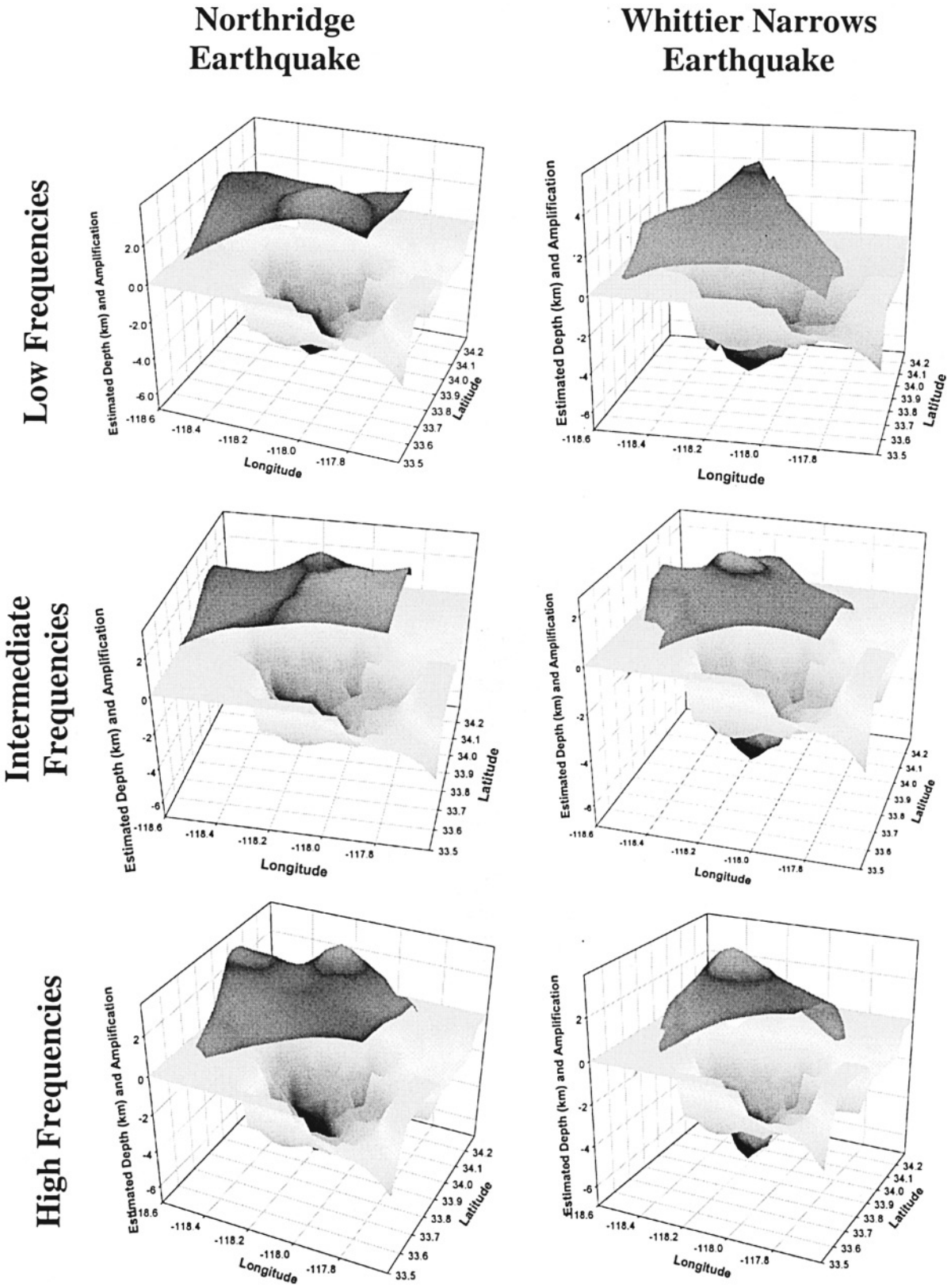

Figure 2. Combined 3D plots of smoothed amplification ratio for each frequency range (upper surface) and of estimated basin depth based on Magistrale *et al.* (2000) (lower surface) for the 1994 Northridge and the 1987 Whittier Narrows earthquakes.

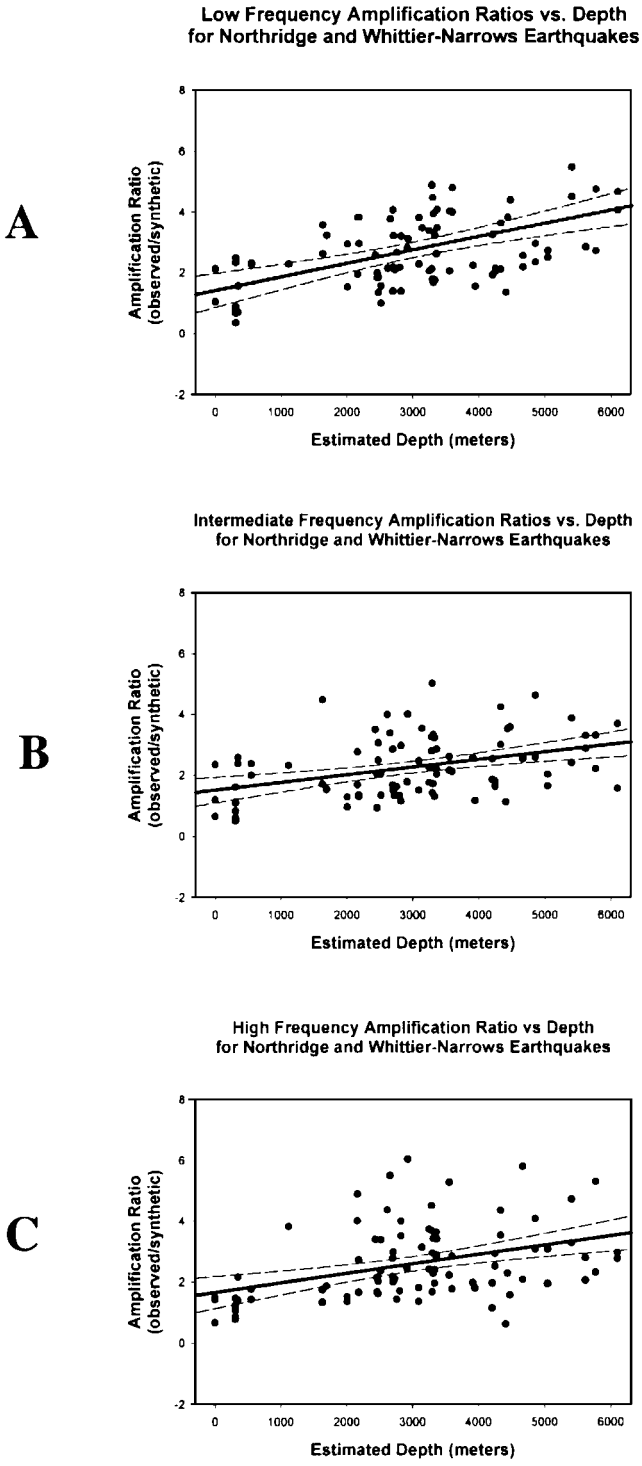

Figure 3. Amplification ratio versus estimated depth based on Magistrale *et al.* (2000) for (A) low frequencies (0.2–2.0 Hz), (B) intermediate frequencies (2.0–8.0 Hz), and (C) high frequencies (8.0–12.5 Hz). All data from Northridge and Whittier Narrows earthquakes are included. In order to make the plots readable and uniform, the amplification ratio for station DWY from the Whittier Narrows earthquake, which is outside the range in plot A, has not been shown; however, it is included in the regression calculation. Dashed lines represent 95% confidence intervals.

Table 3
Regression Equations for Estimating Amplification (A) Based on Depth in Kilometers (d)

	Frequency Range (Hz)	Linear Regression	Correlation Value (r^2)
Low	0.195–2.0	$A = 0.441d + 1.425$	0.25
Intermediate	2.0–8.0	$A = 0.247d + 1.522$	0.15
High	8.0–12.5	$A = 0.309d + 1.660$	0.16
Average	0.195–12.5	$A = 0.289d + 1.563$	0.24

including local resonances at individual sites. The corrections represent the cumulative effect of all these factors and can be viewed as the corrections for the average near-surface condition within the basin, with basin depth as an independent variable. The trend for the correction to increase with depth is well defined on average.

Anderson *et al.* (1996, p. 1749) argued that "the surficial geology has a greater influence on ground motions than might be expected based on its thickness alone." Indeed, the seismic design criteria in the international building codes are based entirely on the National Earthquake Hazards Reduction Program's determinations of the shear-wave velocity of the top 30 m (Mahdyiar, 2002). Clearly, the significance of surface layers cannot be ignored when predicting the site response; however, the amplification predictions based solely on surface geology have been shown to be insufficient. For example, Mahdyiar (2002) concluded that the amplification values based on the shear-wave velocities in the top 30 m did not reflect the basin effects as derived from regional earthquake ground motions (Hartzell *et al.*, 1998).

Mahdyiar's (2002) analysis leads one to conclude that probabilistic seismic hazard analysis would be most successful if both depth-dependent basin effects and the effects of near-surface geology were combined. The SCEC Phase III Working Group came to the same conclusion. It identified two major contributors to the amplification factors: the softness of surface layers and basin depth (Field and SCEC Phase III Working Group, 2000). By calibrating these effects against observed amplifications, SCEC has created an amplification map for the Los Angeles region (www.scec.org/phase3/amplificationmap.html), although the map given at the web site does not provide a technical explanation of how it was constructed. Our amplification corrections are generally comparable spatially and quantitatively to those proposed by the SCEC group. This is of no surprise because both maps are based on the estimation of basin depth by Magistrale *et al.* (2000). However, our maximum amplification correction is near 4, while the SCEC map has a maximum of 5. The source of this inconsistency lies in the way the (non-WWW) published SCEC amplifications (e.g., Field and SCEC Phase III Working Group, 2000, their figure 1) and ours were defined. While the published southern California amplification factors are typically determined based on empirical spectral ratios relative to a single rock site (e.g., Hartzell *et al.*, 1998; Field and SCEC Phase III Working

Group, 2000, their figure 1), our corrections are determined with respect to the average rock-site condition, including many stations, based on finite-fault modeling. The latter can be considered more robust, as these corrections are much less dependent on the choice of a particular rock site.

Our low-frequency (0.2–2 Hz) correction factors, extending to about 4, also compare well with the results of the low-frequency 3D simulations of ground motions within the Los Angeles basin conducted by Wald and Graves (1998) and Olsen (2000) (frequencies below 0.5 Hz in both studies). For example, Wald and Graves (1998) reported the simulated displacement amplitudes about three to four times larger within the basin than at sites outside the basin; Olsen's (2000) scenario-averaged amplification values are up to a factor of 4.

As stated earlier, the corrections introduced in this article can be viewed as those representative of the generic soil condition within the basin, where local site responses have been substantially smoothed out. Clearly, the localized effects, such as a particular site's resonance or focusing due to the geometry of the basin edge, cannot be captured by this generic correction. A sharp local amplification function at any particular site of interest can always be introduced to the program such as FINSIM as an extra input parameter (Beresnev and Atkinson, 1998). Any specifics of local response, if known, can thus be easily incorporated.

Duration

Basin effects have been shown to greatly increase shaking durations. One of the proposed causes for these prolonged durations is the conversion of body waves to surface waves at the basin edges (Bard and Bouchon, 1980a,b, 1985; Vidale and Helmberger, 1988; Joyner, 2000).

For the purposes of this study, the duration is defined as the time from the *S*-wave arrival to the time when 95% of the acceleration spectral energy has passed, which was determined by calculating the squares of the original acceleration traces until 95% of the total was reached. Durations were calculated for both synthetic and observed seismograms for the Northridge and Whittier Narrows earthquakes. For most stations, we averaged the durations of the two horizontal-component seismograms, with the exception of two stations, MBF and XBR, where only one horizontal component for the Whittier Narrows event was available.

As could be expected, the synthetic model significantly underestimates the shaking durations for both earthquake sources, confirming that the Los Angeles basin has a substantial duration effect (see also Olsen, 2000). Durations for the synthetic seismograms range from 7.1 to 12.6 sec for the Northridge event, while the observed durations range from 6.7 to 35.5 sec. In this case, the maximum ratio between the average observed and the synthetic durations is 3.7. On average, the model underestimates durations by a factor of 1.6 for Northridge stations.

For the Whittier Narrows event, the durations of synthetic seismograms range from 3.4 to 5.6 sec, while the observed durations range from 3.3 to 21.7 sec. In this case, the maximum ratio between the average observed and the synthetic durations is 4.3. On average, the model underestimates the Whittier Narrows durations by a factor of 2.3.

Figure 4 shows the ratio of observed to synthetic durations at each station for both the Northridge and Whittier Narrows earthquakes. It is clear that the duration ratios (represented by black circles) do not correlate well with basin depth (represented by shading in Fig. 4). There is, however, some systematic grouping of larger duration ratios within the basin. Joyner (2000) introduced the distance from the basin edge as the distance from the 300-m contour of the depth to crystalline basement to the seismic station along the line connecting the earthquake epicenter to the station. Figure 5 shows that the duration ratios correlate better with the distance from the basin edge as defined by Joyner (2000) than with basin depth; however, a significant scatter is present as for the amplification ratios in Figure 3. It is important to note that we have not limited our study to long-period (low-frequency) surface waves; thus the wave interactions that may contribute to increased durations within the basin in our study are more complex than those explained by Joyner (2000).

Since the Whittier Narrows epicenter was located within the basin (as defined by Magistrale *et al.*, 2000), it becomes difficult to define the distance from the basin edge for this event. Simply by looking at the distribution of duration ratios for both earthquakes in Figure 4, one can see that larger duration ratios are distributed systematically within the basin, but they are very dependent on earthquake location. Thus, we find it impossible to define a generic correction for the effects of the Los Angeles basin on duration; however, we can say with confidence that durations are increased by the basin effects. As a conclusion, users of FINSIM and similar programs should be aware that durations may be extended as much as four times the synthetic ones, depending on the location of the site within the basin.

Conclusions and Recommendation for Future Work

We have isolated the corrections for total basin amplification within the Los Angeles basin that need to be applied to synthetic ground motions generated for the average rock site. The amplification ratios were produced by comparing the observed to the synthetic Fourier spectra created by FINSIM for the 1994 Northridge and 1987 Whittier Narrows earthquakes. The 3D spatial representations indicate the general correlation between the amplification correction and the basin depth while highlighting the significance of two amplification hot spots that occurred during the Northridge event. Sharp local responses are impossible to capture in a generic correction; however, any extra, site-specific amplification can easily be entered into the synthetic models as an input parameter.

The correlation between the amplification and the basin depth as estimated by Magistrale *et al.* (2000) was observed

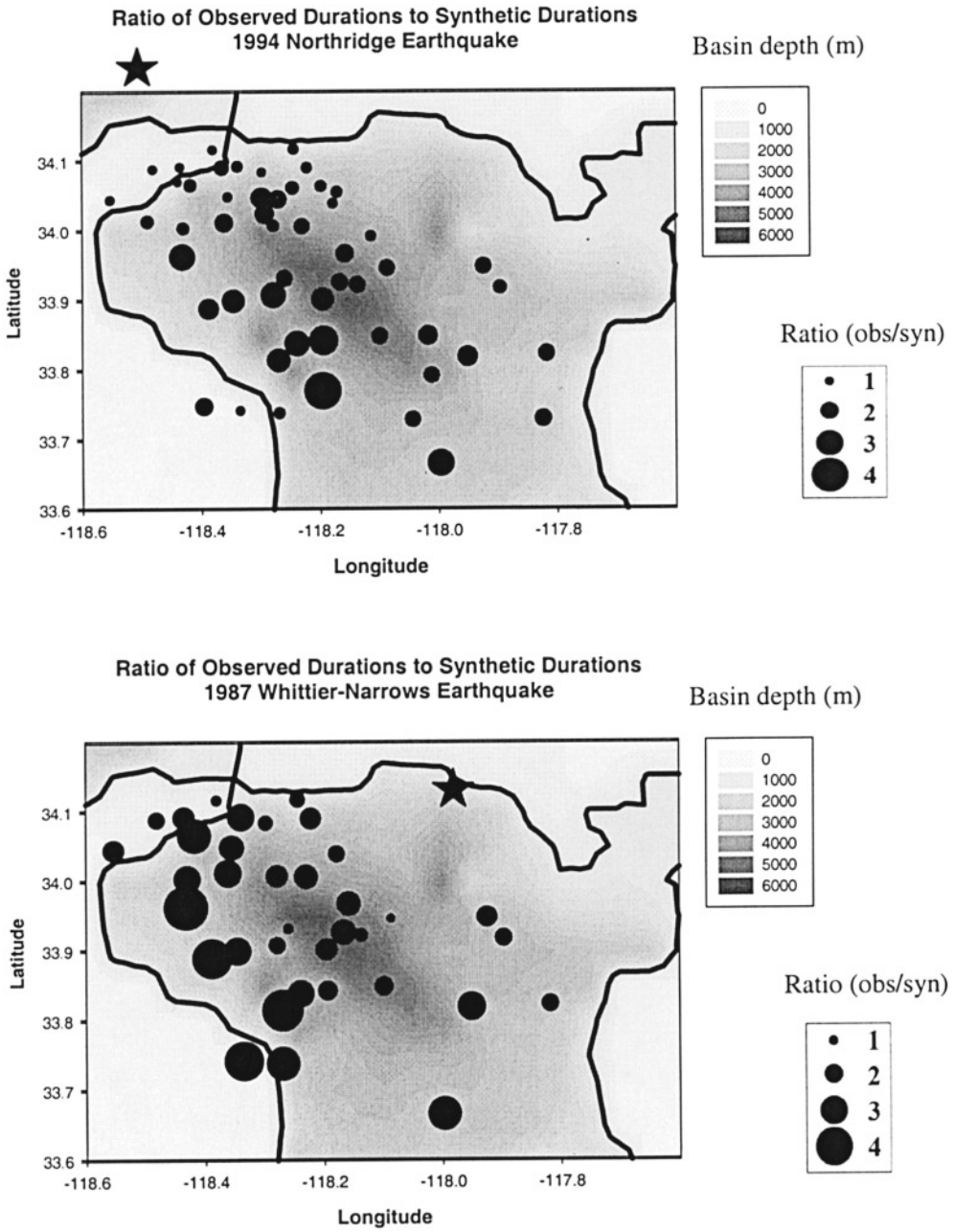

Figure 4. Duration ratios displayed above basin-depth contours (shading) for 1994 Northridge and 1987 Whittier Narrows earthquakes. Black circles are scaled to the ratio values. Stars indicate approximate locations of earthquake epicenters.

in three separate frequency intervals, leading to the development of depth-dependent corrections for the low (0.2–2 Hz), intermediate (2–8 Hz), and high (8–12.5 Hz) frequencies. The correlation coefficients (r^2) below 0.25 indicate significant scatter; however, considering the complexity and local variability of site effects, we consider these correlation factors to be reasonable for the generic correction. The users of FINSIM (or a similar program that does not specifically take the basin structure into account), wishing to generate synthetic ground motions for any site of interest within the basin, should thus proceed as follows. First, the estimated basin depth should be determined from the coordinates of the site using the basin depth calculator (www.scec.org:8081/examples/servlet/BasinDepthServlet). Once the depth has been determined, the equations presented in Table 3 can be used to calculate the amplification factors for the three frequency ranges; these factors should be entered as additional input parameters. This will implement the amplification effect for the generic soil site in the basin. If local resonance is deemed to be significant, a site-specific re-

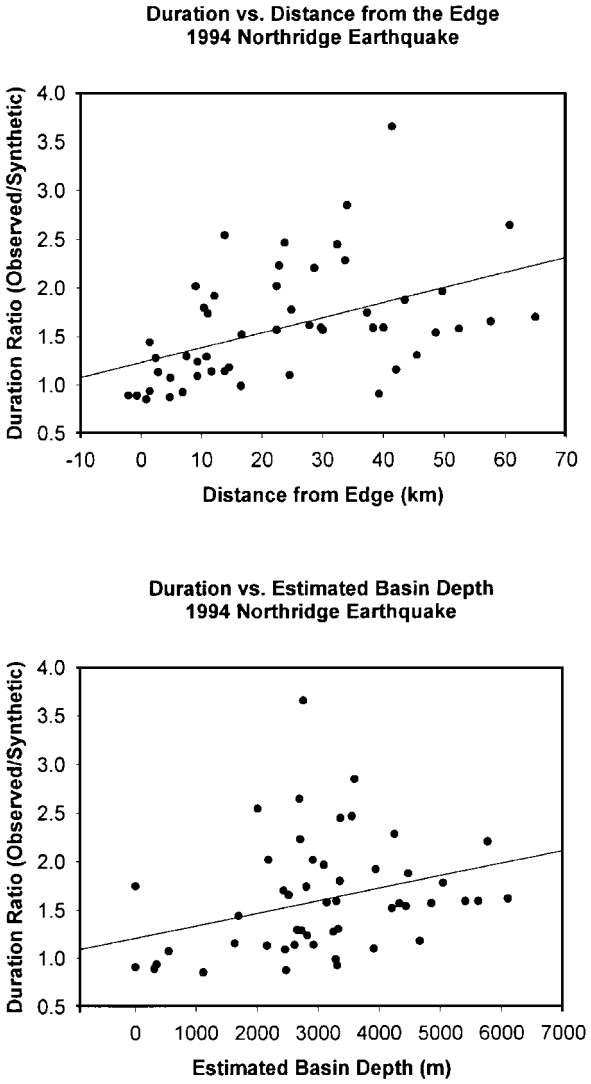

Figure 5. Duration ratios versus distance from the edge (as defined by Joyner, 2000) and versus estimated basin depth for the Northridge earthquake.

sponse function, reflecting the effect of variable near-surface geology, can similarly be incorporated.

Ground-motion durations are shown to be significantly lengthened within the basin. The distance from the edge of the basin is typically considered to be a primary factor affecting the durations (e.g., Joyner, 2000); this distance is ambiguous to define for the epicenters located within basin boundaries. Therefore, it is difficult to make any general prediction or develop corrections concerning duration. Users of non-3D-specific simulation codes should be aware that shaking may occur for as much as four times the length of predicted simulations.

Recently, 3D models have become increasingly popular for evaluating the amplification effects caused by sedimentary basins around the world (Olsen and Archuleta, 1996; Olsen *et al.*, 1997; Pitarka *et al.*, 1998; Wald and Graves, 1998; Stindham *et al.*, 1999; Olsen, 2000). However, these models are limited by the accuracy and resolution of the 3D velocity models on which they depend. Also, they require vast amounts of computer memory and are limited to frequencies typically below 1 Hz. The frequencies of significant engineering interest extend to as high as 20 Hz, which emphasizes the importance of simpler, semiempirical methods, such as the finite-fault stochastic method, for earthquake hazard calculations. The stochastic method, corrected for the average effects of basin structure, as discussed in this article, would be of significant practical use to engineers.

As a result of this study, we have presented corrections for a finite-fault stochastic model, which has been calibrated on rock sites in order to make it effective for sites within the Los Angeles basin. Appropriately modified according to the difference in impedance contrast across the sedimentary cover, these corrections could be used for the other basins as well. However, as we stated in the Introduction, direct portability of these results to other basins should be viewed with caution, since, even for a single Los Angeles basin, the variability in the predicted effect is large (e.g., Fig. 3). The applicability of these predictions elsewhere could only be tested by future earthquake data. Specifically, future work should be directed at determining whether or not these amplification corrections are applicable to other basins. Similar studies must ideally be done in order to develop more basin-specific corrections.

Acknowledgments

This study was supported by Iowa State University. We are grateful to D. Wald for providing elevation data and script used in constructing the map in Figure 1. We are also indebted to F. Chávez-García, D. Boore, and M. Petersen for careful reviews of this manuscript.

References

Alex, C. M., and K. B. Olsen (1998). Lens-effect in Santa Monica? *Geophys. Res. Lett.* **25,** 3441–3444.

Anderson, J. G., Y. Lee, Y. Zeng, and S. Day (1996). Control of strong motion by the upper 30 meters, *Bull. Seism. Soc. Am.* **86,** 1749–1759.

Atkinson, G. M., and W. Silva (2000). Stochastic modeling of California ground motions, *Bull. Seism. Soc. Am.* **90,** 255–274.

Bard, P.-Y., and M. Bouchon (1980a). The seismic response of sediment-filled valleys. I. The case of incident *SH* waves, *Bull. Seism. Soc. Am.* **70,** 1263–1286.

Bard, P.-Y., and M. Bouchon (1980b). The seismic response of sediment-filled valleys. II. The case of incident *P* and *SV* waves, *Bull. Seism. Soc. Am.* **70,** 1921–1941.

Bard, P.-Y., and M. Bouchon (1985). The two-dimensional resonance of sediment-filled valleys, *Bull. Seism. Soc. Am.* **75,** 519–541.

Berardi, R., M. J. Jiménez, G. Zonno, and M. García-Fernández (2000). Calibration of stochastic finite-fault ground motion simulations for the 1997 Umbria–Marche, central Italy, earthquake sequence, *Soil Dyn. Earthquake Eng.* **20,** 315–324.

Beresnev, I. A., and G. M. Atkinson (1998). FINSIM: a FORTRAN program for simulating stochastic acceleration time histories from finite faults, *Seism. Res. Lett.* **69,** 27–32.

Beresnev, I. A., and G. M. Atkinson (2001). Subevent structure of large earthquakes: A ground-motion perspective, *Geophys. Res. Lett.* **28,** 53–56.

Beresnev, I. A., and G. M. Atkinson (2002). Source parameters of earthquakes in eastern and western North America based on finite-fault modeling, *Bull. Seism. Soc. Am.* **92,** 695–710.

Boore, D. M. (1999). Basin waves on a seafloor recording of the 1990 Upland, California, earthquake: implications for ground motions from a larger earthquake, *Bull. Seism. Soc. Am.* **89,** 317–324.

Boore, D., and G. Atkinson (1987). Stochastic prediction of ground motion and spectral response parameters at hard-rock sites in eastern North America, *Bull. Seism. Soc. Am.* **77,** 440–467.

Castro, R. R., A. Rovelli, M. Cocco, M. Di Bona, and F. Pacor (2001). Stochastic simulation of strong-motion records from the 26 September 1997 (M_w 6), Umbria–Marche (central Italy) earthquake, *Bull. Seism. Soc. Am.* **91,** 27–39.

Chávez-García, F. J., and E. Faccioli (2000). Complex site effects and building codes: making the leap, *J. Seism.* **4,** 23–40.

Davis, P. M., J. L. Rubenstein, K. H. Liu, S. S. Gao, and L. Knopoff (2000). Northridge earthquake damage caused by geologic focusing of seismic waves, *Science* **289,** 1746–1750.

Electric Power Research Institute (EPRI) (1993). Method and guidelines for estimating earthquake ground motion in eastern North America, in Guidelines for determining design basis ground motions, Vol. 1, Rept. EPRI TR-102293, Palo Alto, California.

Field, E. H., and the SCEC Phase III Working Group (2000). Accounting for site effects in the probabilistic seismic hazard analyses of southern California: overview of the SCEC Phase III Report, *Bull. Seism. Soc. Am.* **90,** no. 6B, S1–S31.

Gao, S., H. Liu, P. M. Davis, and L. Knopoff (1996). Localized amplification of seismic waves and correlation with damage due to the Northridge earthquake, *Bull. Seism. Soc. Am.* **85,** S209–S230.

Graves, R. W., A. Pitarka, and P. G. Somerville (1998). Ground motion amplification in the Santa Monica area: effects of shallow basin edge structure, *Bull. Seism. Soc. Am.* **88,** 1224–1242.

Hartzell, S, E. Cranswick, A. Frankel, D. Carver, and M. Meremonte (1997). Variability of site response in the Los Angeles urban area, *Bull. Seism. Soc. Am.* **87,** 1377–1400.

Hartzell, S., S. Harmsen, A. Frankel, D. Carver, E. Cranswick, M. Meremonte, and J. Michael (1998). First-generation site-response maps for the Los Angeles region based on earthquake ground motions, *Bull. Seism. Soc. Am.* **88,** 463–472.

Hartzell, S., S. Harmsen, A. Frankel, and S. Larsen (1999). Calculation of broadband time histories of ground motion: comparison of methods and validation using strong-ground motion from the 1994 Northridge earthquake, *Bull. Seism. Soc. Am.* **89,** 1484–1504.

Iglesias, A., S. K. Singh, J. F. Pacheco, and M. Ordaz (2002). A source and wave propagation study of the Copalillo, Mexico, earthquake of 21 July 2000 (M_w 5.9): implications for seismic hazard in Mexico City from inslab earthquakes, *Bull. Seism. Soc. Am.* **92,** 1060–1071.

Joyner, W. B. (2000). Strong motion from surface waves in deep sedimentary basins, *Bull. Seism. Soc. Am.* **90,** no. 6B, S95–S112.

Magistrale, H., S. Day, R. W. Clayton, and R. Graves (2000). The SCEC southern California reference three-dimensional seismic velocity model version 2, *Bull. Seism. Soc. Am.* **90,** no. 6B, S65–S76.

Magistrale H., R. Graves, and R. Clayton (1998). A standard three-dimensional seismic velocity model for southern California: version 1, *EOS* **79,** F605.

Mahdyiar, M. (2002). Are NEHRP and earthquake-based site effects in greater Los Angeles compatible? *Seism. Res. Lett.* **73,** 39–45.

Makra, K., D. Raptakis, F. J. Chávez-García, and K. Pitilakis (2001). Site effects and design provisions: the case of Euroseistest, *Pageoph* **158,** 2349–2367.

Olsen, K. B. (2000). Site amplification in the Los Angeles basin from three-dimensional modeling of ground motion, *Bull. Seism. Soc. Am.* **90,** no. 6B, S77–S94.

Olsen, K. B., and R. J. Archuleta (1996). Three-dimensional simulation of earthquakes on the Los Angeles fault system, *Bull. Seism. Soc. Am.* **86,** 575–596.

Olsen, K. B., R. Madariaga, and R. J. Archuleta (1997). Three-dimensional dynamic simulation of the 1992 Landers earthquake, *Science* **278,** 834–838.

Pitarka, A., K. Irikura, T. Iwata, and H. Sekiguchi (1998). Three-dimensional simulation of the near-fault ground motion for 1995 Hyogo-ken Nanbu (Kobe), Japan, earthquake, *Bull. Seism. Soc. Am.* **88,** 428–440.

Porcella, R. L., E. C. Etheredge, R. P. Maley, and A. V. Acosta (1994). Accelerograms recorded at USGS national strong motion network stations during the M_s = 6.6 Northridge, California earthquake of January 17, 1994, *U.S. Geol. Surv. Open-File Rept. 94-141*, 100 pp.

Roumelioti, Z., and A. Kiratzi (2002). Stochastic simulation of strong-motion records from the 15 April 1979 (*M* 7.1) Montenegro earthquake, *Bull. Seism. Soc. Am.* **92,** 1095–1101.

Shakal, A., M. Huang, R. Darragh, T. Cao, R. Sherburne, P. Malhotra, C. Cramer, R. Sydnor, V. Graizer, G. Maldonado, C. Peterson, and J. Wampole (1994). CSMIP strong-motion records from the Northridge, California earthquake of 17 January 1994, report no. OSMS 94-07, California Strong Motion Instrumentation Program, Sacramento, 308 pp.

Silva, W. J., N. Abrahamson, G. Toro, and C. Costantino (1997). Description and validation of the stochastic ground motion model, report submitted to Brookhaven National Laboratory, Associated Universities, Inc., Upton, New York.

Stindham, C., M. Antolik, D. Dreger, S. Larson, and B. Romanowicz (1999). Three-dimensional structure influences on the strong-motion wavefield of the 1989 Loma Prieta Earthquake, *Bull. Seism. Soc. Am.* **89,** 1184–1202.

Toro, G. R., N. A. Abrahamson, and J. F. Schneider (1997). Model of strong ground motions from earthquakes in central and eastern North America: best estimates and uncertainties, *Seism. Res. Lett.* **68,** 41–57.

Vidale, J. E., and D. V. Helmberger (1988). Elastic finite-difference modeling of the 1971 San Fernando, California, earthquake, *Bull. Seism. Soc. Am.* **78,** 122–141.

Wald, D. J., and R. W. Graves (1998). The seismic response of the Los Angeles basin, California, *Bull. Seism. Soc. Am.* **88,** 337–356.

Department of Geological and Atmospheric Sciences
Iowa State University
253 Science I
Ames, Iowa 50011-3212
chruby@iastate.edu, beresnev@iastate.edu

Manuscript received 21 May 2002.